Geophysica (1998), 34(1-2), 1-21

On the Parameterization of Basal Heat Flux for Sea-ice Modelling

David M. Holland

Lamont-Doherty Earth Observatory of Columbia University
Oceans and Climate Division
P.O. Box 1000, Route 9W, Palisades, New York, 10964, USA

(Received: November 1996; Accepted: March 1997)

Abstract

*A sea-ice model is used to investigate the ice-ocean heat flux that occurs at the base of the ice. The source of this basal heat flux is supposed in reality to arise from physical processes (*e.g. *oceanic mixed-layer entrainment, ocean advection, or solar heating in leads) which elevates the mixed-layer ocean temperature above the* in situ *freezing point and thereby causes a flow of heat from the mixed-layer to the base of the ice. In this study a dynamic-thermodynamic sea-ice model is coupled to a slab ocean model and forced with monthly climatological atmospheric forcing. The model domain is the Arctic Ocean and the neighbouring seas but the focus of the study is the area of perennial Arctic ice away from the marginal ice zones. The question asked, in the context of global climate modelling, is how sensitive is the sea-ice cover to the manner in which the basal heat flux is parameterized. Two numerical experiments are performed using (i) first a procedure in which heat is fluxed from the ocean to the ice using a turbulent transfer parameterization and (ii) secondly a simpler scheme in which heat is transferred instantaneously from the ocean to the ice. The conclusion is that for application in global climate models the simplified scheme (with instantaneous transfer) works satisfactorily. A discussion of the details of the differences in the simulated sea ice for the two experiments is also presented.*

Key words: Arctic oceanography, climate modelling, climate change, ice-ocean heat flux

1. Introduction

Global climate models are becoming more sophisticated in their representation of sea ice. Sea-ice models deemed appropriate for inclusion in such climate models must include some minimum description of ice thermodynamic and dynamic processes. For thermodynamics, this requires that the ice model describe at least two ice thickness categories (i.e. the average ice thickness and the lead fraction) and have a prognostic surface temperature. For dynamics, this requires that the ice be mobile and employ a suitable rheology (e.g. the viscous plastic). Once these essential ingredients are in place it becomes appropriate to ask if refinements to these zero-order thermodynamical and dynamical descriptions are beneficial. For global climate models we must keep in mind

that the goal is to achieve as realistic a representation of the earth's climate by including only those processes which are of fundamental importance. Such an approach is dictated by the limited computing resources available and the need to simplify the climate system as much a possible to enhance understanding. Sensitivity studies using individual component models can aid in identifying the physical process and parameterizations that are most useful for inclusion in fully-coupled multi-component climate models. This paper investigates one important aspect of sea-ice thermodynamics, namely the parameterization of the ice-ocean heat flux that occurs at the base of sea ice. The objective is to determine how to best represent this basal flux in a climate model.

The basal heat originates because the sea-ice base is at the *in situ* freezing point (based on the salinity of the mixed layer) whereas the mixed layer waters are generally at a slightly different temperature. The cause of this disequilibrium ranges from (i) the absorption of shortwave radiation via leads directly into the mixed layer (recall the ocean albedo is approximately 0.07 while that of ice is 0.60), (ii) the advection of warmer open ocean waters into sea ice covered areas or vice versa, to (iii) the upward flow of deeper waters associated with mixed layer entrainment or coastal upwelling. In the instance that the mixed layer is above the freezing point there will be a flux of heat directed toward the base of the ice from the warmer mixed layer. This will cool the mixed layer to the freezing point while at the same time melting some ice.

For the polar regions it is well known that the annually averaged longwave radiation emitted at the top of the atmosphere exceeds the annually averaged absorbed shortwave radiation by about 100 W/m^2 (*Gill*, 1982, p. 2). Almost all of this net radiative heat loss is replenished by horizontal advection of moist static energy (defined as the sum of the sensible heat, latent heat and potential energy) into the polar region from subpolar regions. The residual between the net radiative loss at the top of the atmosphere and the horizontal advective gain represents the net surface flux for the polar regions. For the Arctic this annually averaged net surface flux (see Fig. 1) has been estimated at 2 W/m^2 (*Overland* and *Turet*, 1994). One conclusion to be drawn from this small net residual surface flux is that the surface of the Arctic Ocean is very well insulated from the polar atmosphere by the presence of the sea ice cover.

Unfortunately, because the residual represents such a small heat flux it is difficult to say at present if it is in fact absolutely accurate and furthermore what its source could be. If we take as premise that the Arctic ice cover is in thermodynamic equilibrium then the loss of 2 W/m^2 from the surface must be balanced by some other heat gain in order to maintain equilibrium. Historically, this flux has been taken to represent the heat lost by the Atlantic Layer waters as they circulate cyclonically about the basins of the Arctic Ocean. While en route it has been assumed that they mix vertically with the overlying colder polar waters and thereby effectively produce an upward heat flux. More recently, it has been speculated that the Atlantic Layer may in fact be cooled not by vertical processes but rather by lateral mixing with cold continental shelf waters

(*Aagaard et al.*, 1981). Part of the reasoning for this is the observation that the Arctic Ocean has a halocline extending from the base of the mixed layer to a depth in excess of 200 m. This halocline (i.e. pycnocline) is nearly isothermal and close to the freezing point. It has thus been argued that because the Atlantic Layer waters which lie below the halocline they are very much insulated from processes of vertical exchange with the mixed layer.

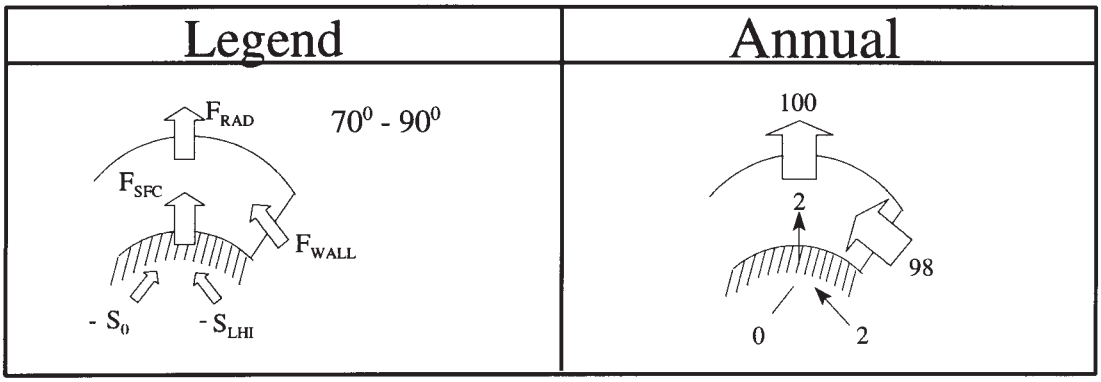

Fig. 1. Schematic representation of the observed poleward energy budget. The left portion of the figure describes the fluxes considered, namely, the radiative F_{RAD}, the northward advection F_{WALL} and the residual surface flux F_{SFC} required for overall energy balance. The surface flux is further broken into a rate of storage of sensible heat into the ocean S_O and the rate of storage of latent heat in sea ice S_{LHI}. The right portion of the figure shows the numerical values of the heat fluxes in W/m^2 annually averaged for the Arctic (after *Overland* and *Turet*, 1994).

More recently the residual surface heat flux has been postulated to arise from the summertime absorption of shortwave radiation into the oceanic mixed layer via the leads (*Maykut* and *Perovich*, 1987). In this scenario the mixed layer heats up above the freezing point and ultimately give rise to turbulent transfer of heat between the mixed layer and the base of the ice.

As an alternative point of view, it can be argued that the residual 2 W/m^2 can be accounted for by the export of ice from the Arctic, principally via Fram Strait. This is seen by considering the net flux of ice through Fram Strait of approximately 0.10 Sv (*Aagaard* and *Carmack*, 1989) and converting this to the equivalent reduction in sea ice thickness averaged over the entire perennially ice-covered Arctic of area 10^{13} m^2. This gives a rate of reduction in ice thickness of

$$\frac{\partial h_{export}}{\partial t} = 10^5 \frac{m^3}{s} / 10^{13} m^2 = 10^{-8} m/s \quad (1)$$

which can be converted into an equivalent basal heat flux Q_{export} of magnitude

$$Q_{export} = \rho_i L_f \frac{\partial h_{export}}{\partial t} = 10^3 \cdot 3 \cdot 10^5 \cdot 10^{-8} = 3 W/m^2 \quad (2)$$

where standard values for the ice density Ψ_i and latent heat of fusion L_f are used. The point here is that the export of ice can by itself wholly account for the net residual surface heat flux required to keep the Arctic in thermodynamic balance.

For uncoupled thermodynamic sea-ice models (without dynamics) it has been the usual practice to prescribe the ice-ocean basal flux as a constant 2 W/m^2 (e.g. *Maykut* and *Untersteiner* 1971, *Semtner* 1976). Because such models lack the ability to transport ice it is understandable that such a prescribed heat flux should be employed in order to achieve a reasonable equilibrium ice thickness. For uncoupled dynamic-thermodynamic sea-ice models no such prescription is required because of the ability to transport ice and also the ability to absorb solar radiation via leads. This paper will show that a realistic ice cover is in fact obtained without the need of a prescribed ice-ocean heat flux. The new research presented shows that for the purposes of climate modelling the absorption of solar radiation through leads is an important contributor to a proper ice simulation but that the details of how this absorbed heat is redistributed from the ocean to the base of the ice is not so important.

The remainder of this paper is organized as follows. Section 2 briefly describes the physics of the dynamic-thermodynamic sea ice model used as well as the slab-ocean mixed layer model and the atmospheric forcing fields. The sensitivity of the simulated sea-ice characteristics to the particular formulation of the ice-ocean basal heat flux are presented in section 3. Section 4 discusses the relevance and the implications of the main results of the paper.

2. *The model*

The model used in this study consists of a dynamic-thermodynamic sea-ice model (*Oberhuber*, 1993) coupled to a slab-ocean mixed-layer model and forced by monthly climatological atmospheric forcing fields. The sea-ice equations are described briefly to highlight the physical processes that are represented. This section ends by describing the physical layout of the model.

2.1 *Sea ice*

For the momentum balance, the ice is considered to move in a two-dimensional spherical plane with forcing fields operating on the ice via simple planetary boundary layers. The nonlinear inertial terms are neglected. The equation is

$$\frac{\partial \vec{u}_i h_i}{\partial t} = \vec{\nabla} \cdot A^m \vec{\nabla} \vec{u}_i h_i - \vec{f} x \vec{u}_i h_i - g h_i \vec{\nabla} \Gamma_o + \frac{\vec{\tau}_a}{\rho_i} + \frac{\vec{\tau}_o}{\rho_i} + \frac{\vec{I}}{\rho_i} \qquad (3)$$

where $\vec{u}_i = (u_i, v_i)$ is the horizontal velocity vector, h_i the ice thickness, A^m the horizontal diffusion coefficient for momentum, $\vec{f}$ the Coriolis vector, g the

acceleration due to gravity, $,_o$ the sea surface dynamic height, Ψ_i the ice density, $\vec{\tau}_a$ the ice surface wind stress, $\vec{\tau}_o$ the ice bottom current stress, and $\vec{I}$ the divergence of the internal ice stress which is based on a viscous-plastic ice rheology (*Hibler*, 1979).

The ice-cover thickness h_i is modelled as continuous nonnegative variable. The presence of leads in the ice is modelled using a variable called the ice concentration q_i and is defined as the fraction of a grid cell area covered by ice; the rest of the cell is covered by open water. The spatial and temporal variations in ice thickness and concentration are modelled by the continuity equations

$$\frac{\partial h_i}{\partial t} = -\vec{\nabla} \cdot (\vec{u}_i h_i) + \vec{\nabla} \cdot A^s \vec{\nabla} h_i + S_h \tag{4}$$

$$\frac{\partial q_i}{\partial t} = -\vec{\nabla} \cdot (\vec{u}_i q_i) + \vec{\nabla} \cdot A^s \vec{\nabla} q_i + S_q \tag{5}$$

where S_h and S_q are thermodynamic forcing or source/sink terms. As this paper is primarily concerned with the thermodynamic aspects of sea ice some attention is given below to the details of these source/sink terms. The numerical diffusion terms for both these scalar equations have the same coefficient A^s.

The source/sink term for the thickness equation is identical to Hibler (1979) which is

$$S_h = F(h_i / q_i) \cdot q_i + F(0) \cdot (1 - q_i) \tag{6}$$

where $F(h_i/q_i)$ is the rate of growth of ice over the ice covered part of a grid cell and $F(0)$ is the growth rate over the leads. Figure 2 shows a plot of this growth rate F as a function of ice thickness. From Eq. (6) it is clear that S_h represents the areal averaged growth rate for a model grid cell. The source/sink term for the ice concentration equation, however, differs between the original *Hibler* (1979) parameterization and the *Oberhuber* (1993) reformulation. It is the difference in the source aspect rather than the sink aspect of S_A that turns out to be of greatest importance. This is because the source term describes the rate at which leads close thereby shutting down the loss of heat from the ocean into the atmosphere that is so crucial to ice growth and the overall annually-averaged ice thickness. Under conditions of ice thickness growth, whereby S_h is positive, the comparative *Hibler* (1979) and *Oberhuber* (1993) formulations for lead closing rates are

$$\begin{aligned} S_q &= F(0) / \hbar_o (1 - q_i) \text{ where } F(0) > 0 \wedge S_h > 0 \text{ (Hibler)} \\ S_q &= S_h / \hbar_o (1 - q_i) \text{ where } S_h > 0 \text{ (Oberhuber)} \end{aligned} \tag{7}$$

The empirical parameter h_o is set to a thickness of 0.50 m (see *Hibler*, 1979, for details) and has a value such that the Hibler model produced a reasonably accurate lead

closing time of about 5 days. Notice that the *Oberhuber* (1993) reformulation is forced not by the growth rate in leads, i.e. not by *F(0)*, but rather by the overall growth rate S_h of ice weighted between the ice covered and ice free regions (refer to Eq. 6). For a typical winter ice cover of thickness 3 m and concentration 99 percent, the Oberhuber formula produces a much slower lead closing timescale than that of Hibler. Since Hibler tuned the parameter $\hbar_o$ to give a lead closing time of about 5 days under winter conditions, it is necessary to retune the $\hbar_o$ parameter for use in the Oberhuber reformulation of S_q. In practice a value of $\hbar_o$ of 0.12 allows the Oberhuber reformulation to closely reproduce the observed lead closing timescale of 5 days of the Hibler parameterization.

The drastic difference in wintertime ice growth rates for thin ice versus thick ice is highlighted in Fig. 2. One can see that for very thin ice the ice growth rates represented by *F(0)* are large and hence cause a fast lead closing time when used in Eqn. (7) in the Hibler formulation. However, when the grid cell average growth rate is used based on an average thickness of 3 m and concentration of 99 percent, then the typical ice growth rate is much smaller and causes a much slower lead closing time when used in Eq. (7) in the Oberhuber reformulation.

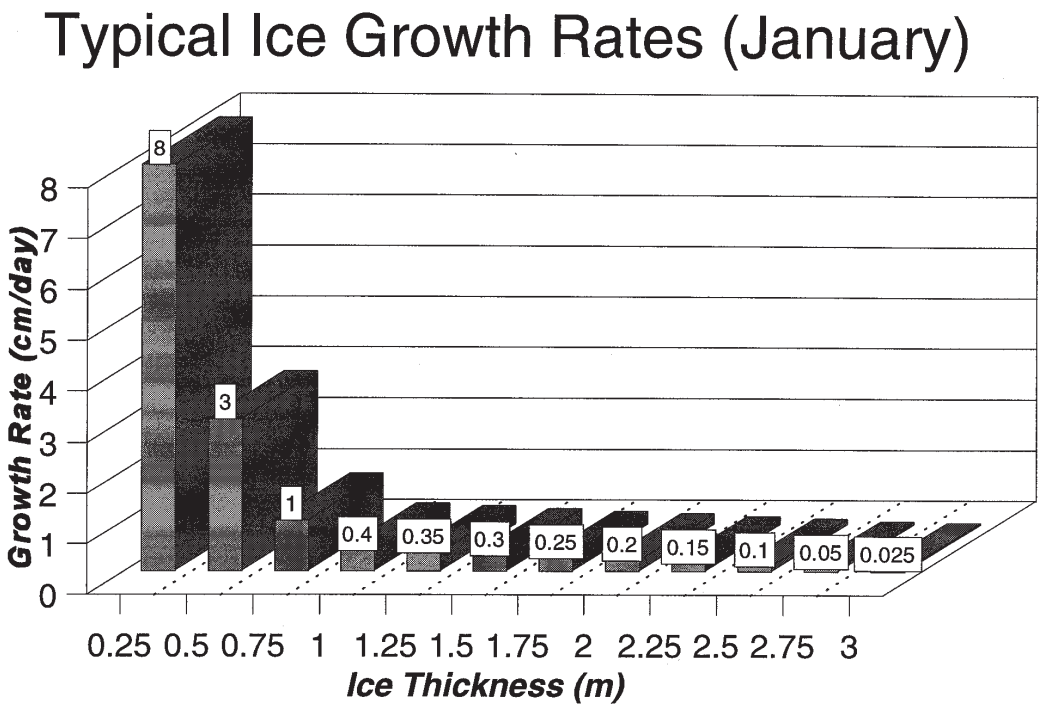

Fig. 2. Typical wintertime (January) sea-ice growth rates (cm/day) as a function of sea-ice thickness (after *Hibler*, 1979).

The thermodynamic description of the sea-ice model is completed by an equation for computing the skin temperature (or equivalently the heat content) of the ice based on the flux divergence of heat between the net atmospheric flux and the ice conductive

flux. The exact details of the algorithm for doing this are outlined in *Oberhuber et al*. (1993) with the one exception that the present study does not involve a snow cover.

2.2 Slab Ocean

The initially prescribed temperature and salinity of the slab ocean are obtained via interpolation of the temperature and salinity data of *Levitus* (1982). Since the freshwater budget of this model is incomplete owing to a lack of adequate precipitation and river run-off data, the slab-ocean salinity is restored to the *Levitus* (1982) climatological salinity using a relaxation time scale of one month. The *in situ* freezing point is salinity dependent according to the relation of *Millero* (1978). The constant depth of the ocean slab is set to 50 m and is denoted by the symbol h_o. Ocean currents $\vec{u}_o = (u_o, v_o)$ are prescribed using output from the *Oberhuber* (1993) ocean general circulation model. A simple advection/diffusion equation is employed for the mixed layer so that heat is advected in the mixed layer according to the prescribed current field. The mixed layer temperature is determined by these advective/diffusive contributions as well as the basal heat flux and the net atmospheric heat flux which occurs through the lead fraction. The heat flux through the leads is denoted Q_{leads} and is the result of carrying out a complete energy balance over the lead part of a grid cell taking into account both the radiative and turbulent heat exchanges. There is no contribution to a change in ocean temperature due to heat conduction through the ice as this process results in an exchange of latent heat for the ocean (i.e. ice growth or melt) and not sensible heat. The equation for the mixed layer temperature T_o is

$$\frac{\partial T_o}{\partial t} = -\vec{\nabla}\cdot(\vec{u}_o h_o) + \vec{\nabla}\cdot A^s \vec{\nabla} h_o + \frac{Q_{basal}}{\rho_o \; c_p \; h_o} + \frac{Q_{leads}}{\rho_o \; c_p \; h_o} \; q_i \qquad (8)$$

where Ψ_o is the density of sea water and c_p is the specific heat.

The atmospheric forcing of the model is achieved using monthly climatological fields of wind stress, radiation, air temperature, humidity, and cloud cover. These fields are described by *Oberhuber* (1988), *Wright* (1988), and *Trenberth et al*. (1989). The model derives the forcing at a particular time step by linearly interpolating between climatological fields of neighbouring months.

2.3 Layout

The domain chosen for this study includes the Arctic Ocean and the Greenland-Iceland-Norwegian (GIN) seas. The model places a solid wall across the outermost boundaries of the domain. The model's geometry is obtained by interpolating a one degree resolution topographic data set onto the model's two degree grid. This coarse resolution captures the basic geometry of the Arctic Ocean and its surrounding land

masses. The resolution of two degrees was chosen to be similar of the typical resolution used in present-day global climate models in their representation of the Arctic region.

A problem with numerical models written in spherical coordinates for the Arctic Ocean is the convergence of the east-west grid spacing near the geographic North Pole. The non-uniformly varying grid spacing near the Pole implies artificially reduced signal speed (*e.g.*, for transports) when an implicit numerical technique, as is done here, is employed. This is overcome by rotating the model coordinates by Eulerian angles such that the model's north pole occurs on the geographical Equator, i.e. the model coordinates are rotated by 90 degrees. All figures presented in this paper indicate the rotated latitude and rotated longitude coordinates along their axes.

3. Sensitivity experiment

In this section two formulations of basal heat flux as presently used in global climate models are described. Simulation results are then presented for an uncoupled sea-ice model using each of the formulations so that an intercomparison can be made.

3.1 Heat flux formulation

The turbulent transfer of heat at the ice-ocean boundary layer has been investigated during a number of observational studies in the Arctic. For instance, the Arctic Ice Dynamics Joint Experiment (AIDJEX), the Marginal Ice Zone Experiment (MIZEX), and the Coordinated Eastern Arctic Experiment (CEAREX) have all contributed, either directly or indirectly, to the collection of data on the transfer of heat between the ocean mixed layer and the base of the ice via small scale eddies. McPhee (1992) has summarized the data from the above experiments. One formulation of basal flux, Q_{basal}, he proposes is

$$Q_{basal} = \rho_o \; c_p \; C_d \; u_* \; (T_{freeze} - T_o) \tag{9}$$

where C_d is the exchange coefficient, u* the friction velocity, and T_{freeze} the *in situ* salinity dependent freezing point. Using typical values (see *McPhee*, 1992) for the various constants and assuming a reasonable friction velocity of 1.0 cm/s and an ocean temperature 0.1 degree above freezing we can estimate the basal flux as

$$Q_{basal} \cong 10^3 \cdot 4 \cdot 10^3 \cdot 5 \cdot 10^{-3} \cdot 10^{-2} \cdot 10^{-1} \cong 20 \; W/m^2 \tag{10}$$

Since this flux is expected to be largely active only for the two months during the summer season when significant shortwave radiation is present, then the annual average flux is reduced to approximately 3 W/m^2. The intention of this scaling is to show that the basal heat flux is also of an appropriate magnitude to close the surface heat budget (refer again to Fig. 1). We must keep in mind that the equivalent heat flux associated with the ice export from Eq. (2) is also of this magnitude. At this point we can not judge

if one or both of the basal and/or the ice export fluxes is actually responsible for maintaining the basin averaged upward surface heat flux of approximately 2 W/m^2 as implied in Fig. 1. There are uncertainties in the estimates proposed by Eqs. (2) and (10) as well as in the observations as summarized by Fig. 1.

The formulation of basal heat flux introduced above will be referred to as the drag law (DL) formulation and is presently employed in global climate models as for example in that of the United Kingdom Meteorological Office, Bracknell (UKMO). An alternative simpler formulation is to instantaneously reset the ocean temperature to the exact freezing point whenever it goes above or below freezing. Accordingly, an appropriate thickness of ice is melted (grown) corresponding to the amount of heat lost (gained) by the ocean to conserve total heat energy. This approach, denoted as the instant relaxation (IR) scheme, is equivalent to specifying an extremely large exchange coefficient, C_d, in place of the typical value of 1.5 x 10^{-3} usually employed. This approach is used for instance in at least one version of the global climate model of the German Max-Planck Institute, Hamburg (MPI).

Depending on the time scale of interest, these two approaches can be quite similar. This is seen by noting that the drag law (DL) formulation as expressed in Eq. (9) implies a time scale for restoration of the ocean temperature exactly back to the freezing point. Considering only changes in the slab-ocean mixed layer arising from the basal flux (i.e. ignoring heat flux through the leads and advective/diffusive contributions) then the heat equation for the slab-ocean temperature (i.e. Eq. (8)) reduces to

$$\rho_o \, c_p \, h_o \, \frac{\partial T_o}{\partial t} \; = \; Q_{basal} \tag{11}$$

Substituting the formulation of basal heat flux from Eqn. (9) into Eq. (11) allows us to determine the relaxation time scale Σ_{DL} for the drag law (DL) formulation as

$$\lambda_{DL} \; = \; \frac{h_{ocn}}{C_d \, u*} \; \cong \; \frac{5 \cdot 10}{1.5 \cdot 10^{-3} \cdot 10^{-2}} \; \cong \; 30 \; days \tag{12}$$

This suggests that on annual and seasonal time scales the two approaches are similar, however, in applications involving ice forecasting over short time intervals of a few days then there would be discrepancy between the two approaches. For such short time intervals the drag law (DL) formulation is more physically based and therefore preferable.

3.2 Drag Law (DL) simulation

The sea ice model is integrated for a five year period starting from initial conditions of no ice. The time series of the modelled domain-averaged ice thickness (Fig. 3a), concentration (Fig. 3b) and ice surface-skin temperature (Fig. 3c) all

approach a cyclo-stationary equilibrium over a seasonal cycle. As an example of the spatial distribution, we show the ice velocity (Fig. 4a), ice thickness (Fig. 4b), ice surface-skin temperature (Fig. 4c) and ice concentration (Fig. 4d) during March of the final year of integration. The velocity pattern (Fig. 4a) is in rough agreement with the general anticyclonic drift as indicated from observations of buoys that have circulated about the Arctic during the last 15 years (*Colony et al.*, 1991). The thickness (Fig. 4b) shows a buildup of ice towards the northern coast of Canada as depicted in the ice thickness charts of *Bourke* and *Garrett* (1987) based on observational data. Additionally, there is a modelled buildup of ice towards Siberia in the region of the Chukchi Sea that is not evident in the Bourke and Garrett data. This is because the modelled ice is very sensitive to the details of the wind forcing employed. The ECMWF winds used did in fact have a bias in producing a flow in the Chukchi Sea region that was directed towards the Siberian coast. The surface skin temperature is also in rough agreement with the temperatures as measured from the buoys which indicate the coldest temperatures of about -32 degrees C off the north coast of Canada (see also Fig. 2.3.10 of the *Gloersen et al*. (1993) atlas). The time series of surface-slab temperature (Fig. 3c) shows that during summer there is a period during which the basin-averaged temperature does reach zero degrees and therefore ice surface ablation ensues. The ice concentration shows a reasonable spatial pattern of the ice edge (Fig. 4d) as well as time series of the seasonal cycle (Fig 3c) when taking into consideration the coarseness of the model horizontal resolution.

An important test of the quality of the ice simulation is its ability to simulate the approximately 0.1 Sv of ice that is exported from the Arctic into the Greenland Sea (*Aagaard* and *Carmack*, 1989). The modelled transport (Fig. 5b) does an adequate job of capturing this feature. The precise model transect line across which the transport is computed is shown separately in Fig. 5a for orientation purposes.

As the parameterized basal flux of Eq. (9) depends upon the ice-ocean friction velocity, Fig. 6d shows a snapshot of the friction velocity during March of the last year of integration. This friction velocity is derived from the difference of the imposed ocean (Fig. 6b) and prognostic ice (Fig. 6c) velocity components. The ice velocity is, as mentioned earlier, largely determined by the wind pattern (Fig. 6a). The friction velocity is computed from the ice-ocean stress $\tau_{i\text{-}o}$ using the relationship

$$\tau_{i\text{-}o} = \rho_o \, u_*^2 \tag{13}$$

and shows as expected an average magnitude of somewhat less that 1.0 cm/s. The largest values occur near the marginal ice zones and in the vicinity of the East Greenland Drift, both places where the ice internal stress is relatively small and the ice is moving rapidly.

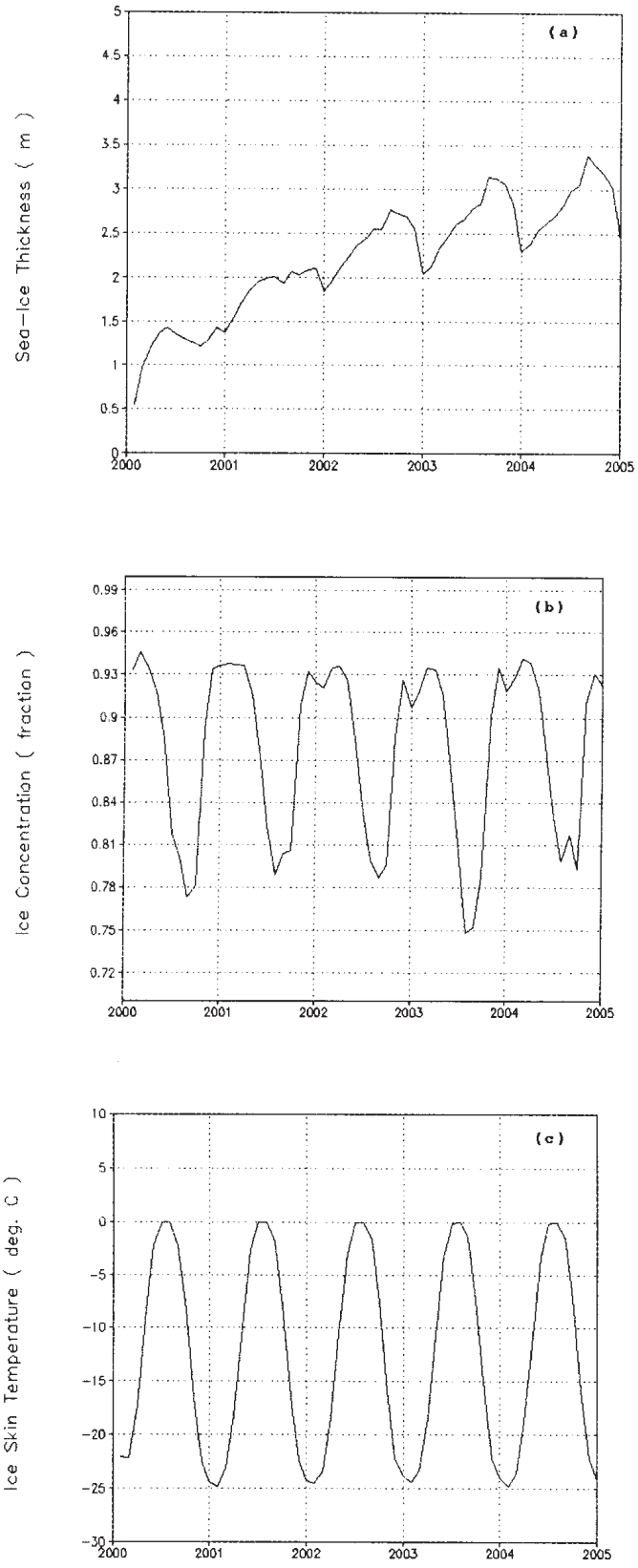

Fig. 3. Time series horizontally averaged over the entire model domain of ice (a) thickness (m), (b) concentration (fraction), and (c) surface skin temperature (°C) for the five year spin up period of the DL experiment.

Fig. 4. Plan view of the ice (a) velocity (cm/s), (b) thickness (m), (c) skin temperature (°C), and (d) concentration (fraction) as a snapshot for March of the final year of integration of the DL experiment. The coastline is indicated by the heavy dotted line. Also the positions of Canada, Greenland and Russia are shown for orientation purposes. Note that the model latitudes and longitudes are rotated by 90 degrees with respect to the true geographical latitudes.

Fig. 5. (a) Plan view of model domain showing the location of the transect line across which the ice transport is computed for the DL experiment. (b) Time series of the volume transport (Sv) of ice exiting the Arctic and flowing into the Nordic seas.

Fig. 6. Plan view of the various winds, ice drifts, and currents used to derive stresses shown for the month of July of the final year of integration for the DL experiment. (a) The imposed surface winds (m/s) over the ocean (the winds over lands are masked out by the grey shading). (b) The imposed ocean surface currents (cm/s). (c) The prognostic sea-ice drift (cm/s). (d) The prognostic net ice-ocean friction velocity (cm/s).

During July the mixed layer temperature (Fig. 7a) is above the freezing point by approximately 0.10 degree in the central Arctic. This is the result of the absorption of shortwave radiation into the leads. The marginal ice zones show a large temperature elevation but they also have their mixed layer temperatures contributed to from the advection of heat by ocean currents in nearby ice free grid cells. In this model run the basal heat flux is computed according to Eq. (9). The resulting heat flux (Fig. 7b) indicates the greatest contribution in the marginal ice zones but also non-negligible (i.e. greater than 1 W/m^2) in the central Arctic.

3.3 Instant relaxation (IR) simulation

The model is rerun for another five year period again starting from an initial condition of no ice but this time the drag law (DL) basal heat flux parameterization is replaced by the simpler instant relaxation (IR) scheme. Despite the fact that the IR run does not employ the heat flux parameterization outlined in Eq. (9) there is nonetheless a basal heat flux. In the IR run as soon as the solar radiation enters the leads it is no longer stored in the ocean as sensible heat but is directly and completely fluxed to the bottom of the sea ice. The result is that the IR basal flux during summer will be greater than the DL scheme because of this instantaneous transfer and there will be a larger summer basal melt for the IR case. Table 1 provides a summary comparing the key statistics for the two runs.

One method for comparison for the two runs is to look at the time series of basal heat flux for the final year of integration. Recall that the DL formulation is dependent upon the friction velocity which we show as a time series (Fig. 8) indicating the friction velocity peaks during fall at which time the winds are strong and the ice internal stresses are relatively small. Both heat flux formulations depend upon the temperature elevations which we compare for the DL (Fig. 9a) versus the IR (Fig. 9b) scheme. The DL scheme, as expected, has a much greater temperature elevation than the IR. The fact that there is any elevation of temperature at all in the IR scheme is the result of the advection of warm water from ice free grid cells into marginal ice zone cells containing ice. Alternatively, the advection of ice into a cell that was previously ice free gives rise to a mixed-layer temperature being not at the freezing point. Finally, comparing the time series of basal flux for the DL (Fig. 10a) versus the IR (Fig. 10b) clearly shows the much greater heat flux associated with the IR scheme. The DL scheme allows for sensible heat stored into the ocean during the summer season to be released back to the atmosphere in the fall (via the leads) without actually affecting ice thickness. In this aspect the two schemes are different, however, it turns out that this difference has negligible impact on the overall ice simulation (i.e. the results presented in Table 1).

Fig. 7. Plan view as a snapshot from July of the final year of integration for the DL experiment. (a) The freezing point elevation (°C) of the ocean mixed layer temperature above the *in situ* freezing point. (b) The turbulent basal heat flux (W/m^2) from the ocean mixed-layer into the base of the sea ice.

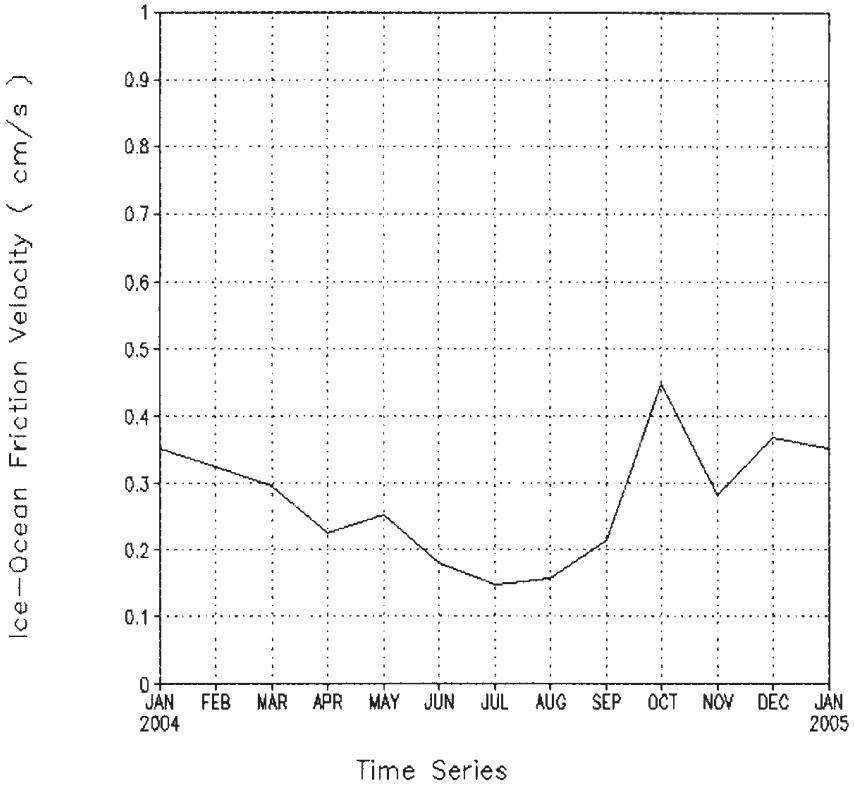

Fig. 8. Time series for the final year of integration (averaged horizontally over the entire model domain) for the DL experiment of the ice-ocean friction velocity (cm/s). Note the IR experiment does not employ an ice-ocean friction velocity for heat transfer and hence no corresponding picture is shown for the IR experiment.

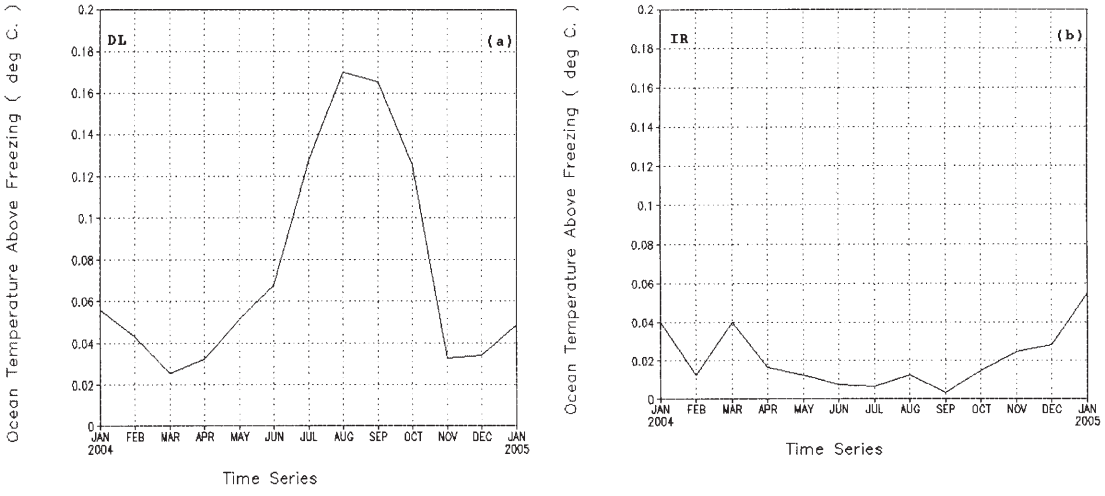

Fig. 9. Time series for the final year of integration (averaged horizontally over the entire model domain) of the freezing point elevation of ocean temperature (°C) for (a) the DL experiment versus (b) the IR experiment.

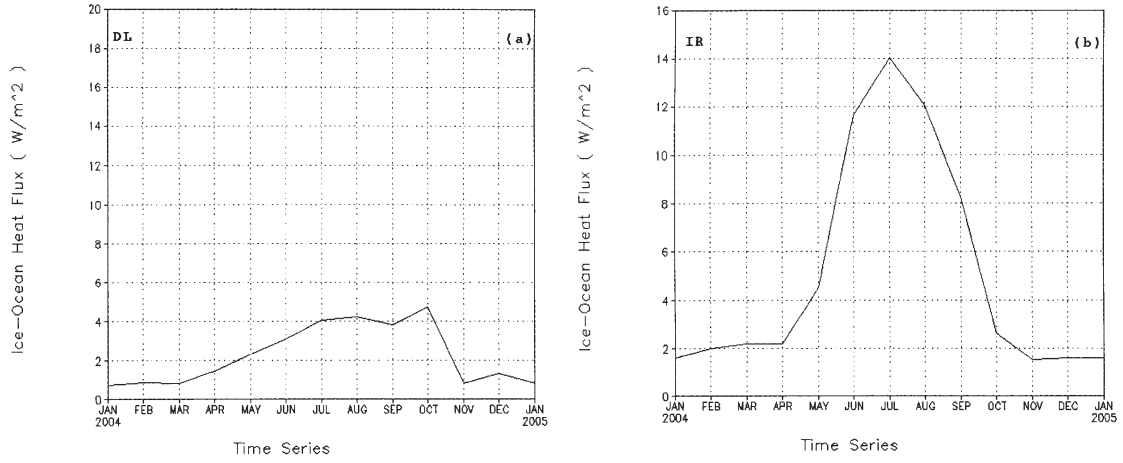

Fig. 10. Time series for the final year of integration (averaged horizontally over the entire model domain) of the turbulent basal heat flux (W/m^2) for (a) the DL experiment versus (b) the IR experiment.

Table 1. Statistical summary of differences in ice-ocean heat flux, ice thickness and ice concentration between the drag law (DL) formulation of ice-ocean heat flux versus that of the instant relaxation (IR) scheme. These calculations are performed on the twelve monthly values for the final year of integration.

	Drag Law (DL) Experiment				**Instant Relaxation (IR) Experiment**			
	Mean	Std. Dev.	Min.	Max.	Mean	Std. Dev.	Min.	Max.
Ice-Ocean Basal Heat Flux	2.43	1.53	0.76	4.75	5.49	4.67	1.54	14.02
Sea-Ice Thickness	3.05	0.36	2.30	3.39	3.04	0.40	2.27	3.34
Sea-Ice Concentration	0.88	0.06	0.79	0.96	0.89	0.04	0.82	0.97

4. Discussion

The key results of the study are now highlighted. A dynamic-thermodynamic sea-ice model coupled to a slab-ocean mixed layer and forced by climatological monthly atmospheric data produced a realistic temporal and spatial pattern of sea-ice cover. The simulated ice velocity, thickness, concentration and surface-skin temperature were all quite reasonable based on the coarseness of the model resolution and the limited observational data base available for comparison. The focus of the paper was not on the details of an extremely accurate simulation but rather on performing a sensitivity study in which two alternate parameterizations of the basal ice-ocean heat flux were described and implemented in the numerical model. The first parameterization was based on turbulent transfer of heat and was referred to as the drag law (DL) scheme while the second used an instantaneous heat transfer (IR). While there were significant

differences in the basal heat flux produced from each parameterization, there was little difference in the overall sea-ice characteristics suggesting that either formulation is appropriate for global climate modelling.

An interesting question to pose is given that the basal heat flux (Table 1) in the IR scheme was on average larger than that of the DL scheme, why was there so little difference in the overall simulated ice characteristics (i.e. thickness and concentration). Part of the explanation is that while the IR scheme provides a greater basal flux during summer and hence a greater summer melt of ice, it also preconditions the water column for earlier freezing during the winter and hence greater winter ice growth. This is because the water column is almost at the freezing point throughout the summer in the IR scheme and subsequently during the fall (when the loss of heat via leads results in ice growth) the ice grows readily without the need to first cool the water column to the freezing point. By contrast, the DL scheme results in the mixed layer temperature being above the freezing point at the end of the summer melt season and subsequently during the fall sensible heat must first be extracted from the mixed layer to cool it to the freezing point before ice growth can commence. In other words, the DL scheme causes part of the surface heat energy to be stored as sensible heat in the mixed layer whereas the IR scheme stores, by comparison, no sensible heat in the mixed layer. The larger summer melt and larger winter growth rates that this implies for the IR scheme compared to the DL is supported by noting from Table 1 that the IR scheme has a greater standard deviation (0.40) of ice thickness growth than that of the DL scheme (0.36).

The overall conclusion from this study is that both the drag law (DL) and the instant relaxation (IR) approaches to computing the ice-ocean basal heat flux work satisfactorily for application in global climate models. The DL has the advantage of being more physically based having been derived from a significant body of observational data. Its use, however, does demand extra computation, for example of the ice-ocean friction velocity, compared to the simpler IR scheme.

Acknowledgements

This work was supported both by a grant from Cray Research Inc. (CRI) and computing facilities provided by the Arctic Region Supercomputing Center (ARSC) at the University of Alaska, Fairbanks.

6. References

Aagaard, K.L., L.K. Coachman and E. Carmack, 1981. On the halocline of the Arctic Ocean, *Deep Sea Res.*, **28**, 529-545.

Aagaard, K., and E.C. Carmack, 1989. The role of sea ice and other fresh water in the Arctic circulation, *J. Geophys. Res.*, **94**, 14,485-14,498.

Bourke, R.H., and R.P. Garrett, 1987. Sea ice thickness distribution in the Arctic Ocean, *Cold Regions Science and Technology*, **13**, 2107-2117.

Colony, R.L., I. Rigor, and K. Runciman-Moore, 1991. A summary of observed ice motion and analyzed atmospheric pressure in the Arctic Basin, 1979-1990, Tech. mem. APL-UW TM13-91, University of Washington, Seattle, Wash., 106 pp.

Gill, A.E., 1982. Atmosphere-Ocean Dynamics, Int. Geophys. Ser., **30**, Academic, San Diego, Calif, 662 pp.

Gloersen, P., W.J. Campbell, D.J. Cavalieri, J.C. Comiso, C.L. Parkinson, and H.J. Zwally, 1992. Arctic and Antarctic Sea Ice, 1978-1987: Satellite Passive-Microwave Observations and Analysis, NASA SP-511, Washington D.C., 290 pp.

Hibler, W.D. III, 1979. A dynamic thermodynamic sea-ice model, *J. Phys. Oceanogr*., **9**, 815-846.

Levitus, S., 1982. Climatological atlas of the world ocean, NOAA Publ. **13**, U.S. Dept. of Commerce, Washington, D.C., 173 pp.

Maykut, G.A., and N. Untersteiner, 1971. Some results from a time dependent, thermodynamic model of sea ice, *J. Geophys. Res*., **76**, 1550-1575.

Maykut, G.A. And D.K. Perovich, 1987. The role of Shortwave radiation in the summer decay of a sea ice cover, *J. Geophys. Res*., **92**, 7032-7044.

McPhee, M.G., 1992. Turbulent heat flux in the upper ocean under sea ice, *J. Geophys. Res*., **97**, 5365-5379.

Millero, F.J., 1978. Freezing point of sea water, Eigth report of the Joint Panel on Oceanographic Tables and Standards, UNESCO, Tech. Pap. In Mar. Sci., **28**, 1 Annex 6, UNESCO, Paris.

Oberhuber, J.M., 1988. An atlas based on the COADS data set: The budgets of heat, buoyancy, and turbulent kinetic energy at the surface of the global ocean, Max-Planck-Institute for Meteorology, Hamburg, Report **15**, 199 pp.

Oberhuber, J.M., 1993. Simulation of the Atlantic circulation with a coupled sea ice - mixed layer - isopycnal general circulation model, Part I: Model Description, *J. Phys. Oceanogr.*, **23**, 808-829.

Oberhuber, J.M., D.M. Holland, and L.A. Mysak, 1993. A thermodynamic-dynamic snow sea-ice model, Ice in the climate system, NATO ASI Series, Series I: Global Environmental Change, W.R. Peltier (ed.), 653-673.

Overland, J.E., and P. Turet, 1994. Variability of the atmospheric energy flux across 70 N computed from the GFDL data set, In: Polar Oceans and their Role in Shaping the Global Environment, ed. O. M. Johannessen, R.D. Muench and J.E. Overland, American Geophysical Union, Washington, D.C., 525 pp.

Semtner, A.J., Jr., 1976. A model for the thermodynamic growth of sea ice in numerical investigations of climate, *J. Phys. Oceanogr*., **6**, 379-389.

Trenberth, K.E., J.G. Olson, and W.G. Large, 1989. A global ocean wind stress climatology based on ECMWF analyses, NCAR Technical Note, NCAR/TN-338-STR, Boulder, Colorado.

Wright, P., 1988. An atlas based on the COADS data set: Fields of mean wind, cloudiness, and humidity at the surface of the global ocean, Max-Planck-Institute for Meteorology, Hamburg, Report **14**, 70 pp.